

# A boundary integral method applied to the 3D water coning problem

S. K. Lucas

School of Mathematics  
University of South Australia  
The Levels, SA 5095  
Australia

A. Kucera

School of Finance and Economics  
University of Technology, Sydney  
PO Box 123 Broadway, NSW 2007  
Australia

Submitted November 1995, Revised June 1996,  
to *Physics of Fluids*

## Abstract

Often in oil reservoirs a layer of water lies under the layer of oil. The suction pressure due to a distribution of oil wells will cause the oil-water interface to rise up towards the wells. A three-dimensional boundary integral formulation is presented for calculating the steady interface shape when the oil wells are represented by point sinks. Sophisticated integration techniques are implemented in an effort to obtain accurate results. In particular, the efficiency of various integration methods are compared for this problem, including QUADPACK routines, adaptive methods based on the IMT rule, the Kronrod rule, the method of degenerate quadrilaterals, and the Gauss-Rational rule for infinite integrals. Numerical results for various general multi-sink distributions are discussed, as are some further results for the axisymmetric single well problem.

## Keywords:

Water-coning, Oil-well, Interface, 2d integration

## Subject classifications:

65R20 - Integral equations

76S05 - Flow in porous media

## Abbreviated title:

A BIM applied to 3D water coning

# 1 Introduction

Typically, when oil is trapped in a reservoir of porous rock by impermeable layers, a layer of water is found beneath (Muskat [25], Bear [2]). When the oil is drained from the reservoir by a drilled oil well, the pressure gradient generated will cause the oil-water interface to rise; the distortion of the oil-water interface is counterbalanced by gravity forces due to density differences. Depending on the magnitude of the forces, the oil-water interface may reach a stable shape below the well, or reach the well, causing the undesirable product of pumping a mixture of oil and water to the surface. This rising and possible breakthrough to the well of the water layer is known as “water coning” in an oil reservoir.

Fluid movement in porous media has been extensively analysed by models with a modified Darcy’s law, using relative permeabilities and saturations. For a detailed discussion concerning the engineering aspects of the problem we recommend Hinch [13], which explains some of the processes involved and the typical magnitudes of the quantities relevant to the fluid mechanics in a simple and easily understood manner. Bear and Dagan [3] studied axisymmetric interface problems using the hodograph method, and recently, McCarthy [24] presented further extensions to coning problems using similar techniques. The objective of this paper is to use a Darcy’s law model for flow in porous media ([2], [25]) and the associated boundary integral formulation to obtain the steady state shape of the oil-water interface due to the influence of more than one oil well. This is an extension of the work of Lucas *et al.* [23], where the axisymmetric case of a single well or vertical line of wells was examined. To the best of our knowledge the numerical solution reported here for the water coning problem is the first to present three-dimensional interface shapes.

The motion of an interface between two immiscible or density-stratified fluids where one is being withdrawn is a topic not limited to porous media models. The free surface position for the similar inviscid potential-flow problem has been investigated in for example Tuck and Vanden-Broeck [29] and Hocking [14, 15]. Withdrawal from a viscous two-layer system has also been investigated by Lister [22]. Again, these formulations have either been two-dimensional or axisymmetric, and unable to deal with more general sink distributions.

Over the last two decades the boundary integral method has received a great deal of attention from researchers working in such diverse fields as numerical analysis, fluid dynamics, soil dynamics, and almost all of the many engineering disciplines. Reviews can be found in, for example, Beskos [4] and Brebbia *et al.* [6], with hundreds of references to scientific and technical journal articles. The boundary integral method replaces the field equation with an appropriate integral equation, and thereby reduces the dimension of the problem. Problems with wholly Dirichlet or Neumann boundary conditions lead to integral equations of the first or second kind respectively, while problems with different types of boundary conditions on different portions of the boundary lead to a mixed integral equation.

When an engineering or physics problem is posed as an integral equation, it is usually solved numerically. The boundary integral method involves discretizing the boundary

into a number of elements, typically approximating the unknown functions by low order polynomials, and inverting the resultant system of linear equations (the boundary element method). Despite the large amount of work already done in developing the boundary integral method, there have been relatively few applications of the method to fully three-dimensional free-boundary problems. In the work that has been performed, the surfaces in question are usually discretized into a finite number of flat boundary elements, and the unknown functions assumed constant over them. While constant elements are by far the most straightforward to implement numerically, more sophisticated methods are computationally more efficient. For example, Coleman *et al.* [8] and Ramia *et al.* [27], among others, make use of quadratic element approximations of both the surface and unknowns, while more recently Higdon and Muldowney [12] use a spectral discretization over elements.

Here the three-dimensional water coning problem associated with the recovery of oil from underground reservoirs is investigated, which leads to the formulation and solution of an integral equation of the second kind for the unknown interface height. Using previously obtained numerical solutions for the axisymmetric coning problem as a starting point (Lucas *et al.* [23]) an efficient iterative numerical scheme is developed. Employing bicubic splines rather than constant or linear elements, coupled with sophisticated two-dimensional integration routines, we show that our three-dimensional scheme returns the same solutions as obtained when one exploits the axial symmetry for the associated two-dimensional problem. Results are also presented concerning the accuracy and the convergence rate of this method. Wherever relevant, comparisons are made between the performances of two- and the three-dimensional codes. In doing so, the effectiveness and stability of the method are demonstrated.

Results are presented for the steady state height of the interface between oil and water in full three-dimensional simulations of multi-sink distributions. These could be of interest to the oil industry, at least giving qualitative information on multi-sink interactions.

## 2 Governing equations

Consider as a model for porous rock an isotropic homogeneous medium of constant permeability  $k$  which occupies all space. Assume the space is filled with either oil or water, and that there is a sharp interface (justified in Bear [2]) between the two fluids, as shown in Figure 1. We can then apply Darcy's law independently to both regions, where fluid viscosities and densities are different. The oil well(s) are modelled by point sink(s) within the oil layer.

Assume that the upper fluid (oil) has density  $\rho_1$  and viscosity  $\mu_1$ , and the lower fluid (water) has density  $\rho_2 (> \rho_1)$  and viscosity  $\mu_2$ . The fluids are separated by an interface denoted by  $z = \zeta(x, y, t)$ . Darcy's law applied to both fluids gives

$$\mathbf{u}^{(i)} = -\frac{k}{\mu_i} \nabla \hat{p}^{(i)} \quad \text{for } i = 1, 2, \quad (2.1)$$

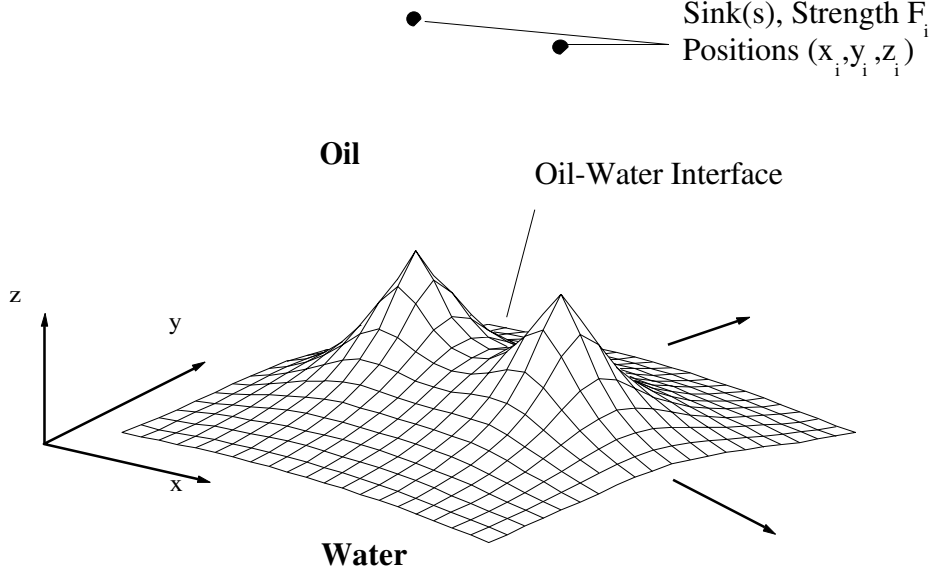


Figure 1: The geometry of the water coning model in 3D.

where

$$\hat{p}^{(i)} = p^{(i)} + \rho_i g z \quad (2.2)$$

is the modified pressure,  $\mathbf{u}^{(i)}$  is the velocity,  $\mu_i$  the viscosity, and  $\rho_i$  the density. The background reservoir pressure is assumed zero. The addition of this term, in any event, is trivial. The incompressibility condition in both fluids is

$$\nabla \cdot \mathbf{u}^{(i)} = 0, \quad (2.3)$$

which, when taken with (2.1), gives Laplace's equation for the modified pressures as

$$\nabla^2 \hat{p}^{(i)} = 0, \quad (2.4)$$

with the boundary condition that  $\mathbf{u}^{(i)}$  and hence  $\hat{p}^{(i)}$  tends to zero at infinity. Note that equation (2.3) for the modified pressure assumes no point sinks in space. We also have dynamic and material boundary conditions on the interface as respectively

$$\begin{aligned} \text{(a)} \quad & p^{(1)} = p^{(2)}, \\ \text{(b)} \quad & \frac{\partial \zeta}{\partial t} + \mathbf{u} \cdot \nabla (\zeta - z) = 0, \quad \text{on } z = \zeta(x, y, t), \end{aligned} \quad (2.5)$$

where  $\mathbf{u}$  is the velocity of the interface. Finally, a specification of the sink strength is required. Here, an oil well is modelled as a point sink of volume flow rate  $m$ . Using the convention that  $m > 0$  for flow into the sink, and with (2.1), the expression for the suction pressure in an infinite porous medium is

$$p_s = \frac{-m\mu_1}{4\pi k((x-x')^2 + (y-y')^2 + (z-z')^2)^{1/2}}, \quad (2.6)$$

where the sink is in the upper fluid at position  $(x', y', z')$ . It is assumed here that the plane  $z = 0$  is the position of the oil-water interface far from the sink, or, the position of the oil-water interface if there is no well in operation. Since we are considering a

steady state solution, an initial shape is not required, and  $\partial p/\partial n = 0$  can be specified on the boundary, as we require the boundary to be static at the steady state. This also implies that  $\hat{p}^{(2)} = 0$ , since the steady state problem requires no flow in the lower fluid. In addition, the kinematic boundary condition (2.5b) becomes identically zero.

Working in the upper fluid, and so dropping the superscript, the form of the dynamic boundary condition (2.5a) using (2.2) is

$$g\zeta(\rho_2 - \rho_1) + \hat{p} = 0 \quad \text{on} \quad z = \zeta(x, y). \quad (2.7)$$

Note that the steady state problem implies that  $z = \zeta(x, y)$ . By scaling lengths with respect to  $z'$ , and pressure with respect to  $m_0\mu_1/kz'$ , where  $m_0$  is a typical sink strength, and choosing  $m_0 = \mu_1/gz'^2(\rho_2 - \rho_1)k$ , the dimensionless form of the dynamic boundary condition (2.7) can be rewritten as

$$\tilde{\zeta} + \tilde{p} = 0 \quad \text{on} \quad \tilde{z} = \tilde{\zeta}(\tilde{x}, \tilde{y}), \quad (2.8)$$

where  $\tilde{\zeta}$  and  $\tilde{p}$  are dimensionless interface height and dynamic pressure respectively. This implies that the sink is at the (dimensionless) point  $(\tilde{x}', \tilde{y}', 1)$ , and that (2.6) becomes, in dimensionless form,

$$\tilde{p}_s = \frac{-F}{4\pi\sqrt{(\tilde{x} - \tilde{x}')^2 + (\tilde{y} - \tilde{y}')^2 + (\tilde{z} - 1)^2}}, \quad (2.9)$$

where

$$F = \frac{m\mu_1}{kz'^2(\rho_2 - \rho_1)g} \quad (2.10)$$

is the only dimensionless parameter that appears in the problem, and represents a balance between the suction force of the sink and the gravitational restoring force of the denser fluid. Thus, we are interested in solving

$$\nabla^2 p = -F\delta(\mathbf{x} - \mathbf{x}'), \quad (2.11)$$

where the tildes have from here on been removed from all dimensionless quantities, and  $\delta$  is the Dirac delta function acting at position  $\mathbf{x}'$  representing an oil well.

### 3 Boundary Integral Formulation

For a smooth function  $\phi$  that satisfies Laplace's equation in a domain  $\Omega$  with smooth surface  $S$ , Green's integral formula says that

$$c\phi(\mathbf{x}_0) + \int_S \phi(\mathbf{x}) \frac{\partial G(\mathbf{x}_0, \mathbf{x})}{\partial n} dS(\mathbf{x}) = \int_S \frac{\partial \phi(\mathbf{x})}{\partial n} G(\mathbf{x}_0, \mathbf{x}) dS(\mathbf{x}), \quad (3.1)$$

where  $\mathbf{x}_0 \in \Omega + S$ ,  $\mathbf{x} \in S$ ,

$$c = \begin{cases} 1 & \mathbf{x}_0 \in \Omega, \\ 1/2 & \mathbf{x}_0 \in S, \end{cases} \quad \text{and} \quad G(\mathbf{x}_0, \mathbf{x}) = \frac{1}{4\pi|\mathbf{x}_0 - \mathbf{x}|}. \quad (3.2)$$

For the water-coning problem there is a forcing term, which involves a volume integral in the formulation of Green's integral formula. Due to the form of (2.11), (3.1) is expressed as

$$cp(\mathbf{x}_0) = p_s(\mathbf{x}_0) + \int_S \left( \frac{\partial p(\mathbf{x})}{\partial n} G(\mathbf{x}_0, \mathbf{x}) - p(\mathbf{x}) \frac{\partial G(\mathbf{x}_0, \mathbf{x})}{\partial n} \right) dS(\mathbf{x}), \quad (3.3)$$

where  $\mathbf{x}_0 \in \Omega + S$  and  $\mathbf{x} \in S$ . The region  $\Omega$  is the upper fluid (oil). At steady state,  $\partial p / \partial n = 0$  along the interface. Multiplying (3.3) throughout by  $-1$  and applying (2.8) leads to the representation of the unknown interface shape as

$$\frac{1}{2}\zeta(x_0, y_0) = -p_s(x_0, y_0) - \int_S \zeta(x, y) \frac{\partial G}{\partial n}(x_0, y_0, x, y) dS(x, y), \quad (3.4)$$

where  $S$  is the surface

$$z - \zeta(x, y) = 0 \quad \text{for } x, y \in (-\infty, \infty), \quad (3.5)$$

with the outward normal directed into the lower fluid, while the Green's function  $G$  is given by

$$G = \frac{1}{4\pi\sqrt{(x-x_0)^2 + (y-y_0)^2 + (z-z_0)^2}}. \quad (3.6)$$

Note that (2.8) can only be used on the unknown surface,  $\zeta$ , hence the value of  $c = 1/2$ . Also, the surface (3.5) does not include the boundary on the oil at infinity because its contribution to the integral in (3.1) is zero.

The derivation of the water coning problem up to now has assumed one point sink of strength  $m$  at position  $(x', y', 1)$  in the upper (oil) region. The addition of further sinks for a more general model is straightforward. Having several sinks, each of dimensionless sink strength  $F_i$  on the right-hand side of (2.11) leads to a sum of terms in  $p_s$ , such that

$$-p_s(x_0, y_0) \equiv \frac{1}{4\pi} \sum_{i=1}^N \frac{F_i}{\sqrt{(x_0-x'_i)^2 + (y_0-y'_i)^2 + (z_0-z'_i)^2}}, \quad (3.7)$$

where there are  $N$  sinks of strengths  $F_i$  at positions  $(x'_i, y'_i, z'_i)$ .

With the surface defined by (3.5), the unit normal (downwards) is

$$\mathbf{n} = -\frac{\nabla F}{|\nabla F|} = \frac{(\partial\zeta/\partial x, \partial\zeta/\partial y, -1)}{\sqrt{(\partial\zeta/\partial x)^2 + (\partial\zeta/\partial y)^2 + 1}}. \quad (3.8)$$

Using (3.6) and (3.8) we get that

$$\frac{\partial G}{\partial n} = \mathbf{n} \cdot \nabla G = \frac{-\frac{\partial\zeta}{\partial x}(x-x_0) - \frac{\partial\zeta}{\partial y}(y-y_0) + (z-z_0)}{4\pi [(x-x_0)^2 + (y-y_0)^2 + (z-z_0)^2]^{3/2} \sqrt{\left(\frac{\partial\zeta}{\partial x}\right)^2 + \left(\frac{\partial\zeta}{\partial y}\right)^2 + 1}}. \quad (3.9)$$

Mapping the surface (3.5) onto the  $xy$  plane, and using (3.7), (3.8) and (3.9) in (3.4), the equation for the unknown interface position is derived as

$$\begin{aligned} \frac{1}{2}\zeta(x_0, y_0) &= \frac{1}{4\pi} \sum_{i=1}^N \frac{F_i}{\sqrt{(x_0-x'_i)^2 + (y_0-y'_i)^2 + (\zeta(x_0, y_0) - z'_i)^2}} \\ &+ \frac{1}{4\pi} \int_{-\infty}^{\infty} \int_{-\infty}^{\infty} \frac{\zeta \left( \frac{\partial\zeta}{\partial x}(x-x_0) + \frac{\partial\zeta}{\partial y}(y-y_0) - (\zeta(x, y) - \zeta(x_0, y_0)) \right)}{[(x-x_0)^2 + (y-y_0)^2 + (\zeta(x, y) - \zeta(x_0, y_0))^2]^{3/2}} dx dy \end{aligned} \quad (3.10)$$

for the case of  $N$  sinks.

## 4 Solution method

Equation (3.10) for the unknown interface is a nonlinear integral equation of the second kind. It is solved by a method similar to that of Lucas *et al.* [23], except a three-dimensional problem is being solved as opposed to an axisymmetric one. Equation (3.10) is solved by a fixed-point iteration technique, starting with the first order small parameter approximation (see Section 4.1) as an initial approximation  $\zeta^0$ , which is substituted into the right-hand side of (3.10) to find the next function  $\zeta^1$  as the left-hand side. This process is repeated, and generates a sequence of surfaces  $\{\zeta^n\}_{n=1}^{\infty}$ , that converges pointwise to  $\zeta$ , the final steady interface solution. The method involves forming a grid of  $(x_0, y_0)$  points in the rectangle defined by

$$-x_{\max} < x < x_{\max}, \quad -y_{\max} < y < y_{\max}, \quad (4.1)$$

evaluating the integrals at these points, and updating the interface height on these grid points until convergence is reached. Outside of the region defined by (4.1), the small parameter solution will be assumed for the interface height (Section 4.1). In all cases examined here, it was found that  $x_{\max} = y_{\max} = 5$  was satisfactory.

Equation (3.10) is singular at  $(x, y) = (x_0, y_0)$ . Often, a process of desingularisation leads to a formulation which relatively simple integration techniques; write  $\zeta(x, y) = (\zeta(x, y) - \zeta(x_0, y_0)) + \zeta(x_0, y_0)$ , and deal with the integral multiplying the last term analytically. Unfortunately, the nonlinearity of (3.10) means such an approach will be unsuccessful. Even for linear integral equations formed using boundary integral techniques, if the unknown function is represented by other than piecewise linear elements, singular integrals are difficult to deal with analytically (see Brebbia *et al.* [6]).

Equation (3.10) involves not only the unknown  $\zeta$ , but also both of its partial first derivatives. Since reasonable integration schemes require more points than just the given node points, an efficient interpolation procedure is required to give acceptable convergence of the solution based on the point grid density. A bicubic spline based on that described in de Boor [9] for function values between points is used. This bicubic spline requires function values at mesh points, as well as the function's normal derivatives at the mesh boundaries, as well as the function's second derivatives with respect to both  $x$  and  $y$  at the corners of the mesh. The derivative data on the boundary of the mesh is supplied by the small parameter solution.

To solve (3.10), the plane  $x, y \in (-\infty, \infty)$ , over which the interface needs to be found, is divided into that in (4.1), which will be called the *inner region*, and the rest of the plane, denoted the *outer region*. In this outer region, the small parameter approximation is used for  $\zeta$ , and so the relatively simple 2D Gauss-Rational scheme for integration can be used (see Appendix A.1). Slight adjustments are required when the node point  $(x_0, y_0)$  for which integration is performed is near the boundary of the outer region, as described in Section 4.2. In the inner region, there is the complication of a singularity in the integrand at  $(x, y) = (x_0, y_0)$ . This singularity was initially handled by using the QUADPACK numerical integration package of Piessens *et al.* [26]. By using two copies of the 1D DQAGS routine, a two-dimensional integrator was set up which can successfully integrate a region with a singularity on the boundary; of course the singularity has to be integrable for convergence by any numerical integral scheme. This

method was implemented by splitting the inner region into  $(-x_{\max} \leq x \leq x_{\max}, -y_0 \leq y \leq y_{\max})$  and  $(-x_{\max} \leq x \leq x_{\max}, -y_{\max} \leq y \leq y_0)$ . However, this procedure was judged to be inefficient, as is the case whenever a general 1D integration technique is extended to 2D and used for more complex integrals, such as those required in solving (3.10) (e.g. see Figure 17). To improve computational efficiency, the IMT rule (Appendix A.2) and a general 2D adaptive integration scheme (Appendix A.4) was implemented in the inner region. While this produces more efficient code than the QUADPACK implementation, we observed some problems with convergence for the IMT rule. As a result, an adaptive method based on triangular elements, using degenerate quadrilaterals to deal with a point singularity, was developed, as described in Appendix A.3. The integration routine developed is called Tri-208 ahead, indicating a rule for integrating over triangles which uses 208 quadrature points. Details of the implementation of these schemes for solving (3.10) is described in Section 4.2.

## 4.1 The small parameter expansion

Blake and Kucera [5] considered the axisymmetric flow due to a single sink and derived a regular asymptotic expansion, based on small  $F$ , for the interface shape. They obtained the first order axisymmetric solution

$$\zeta_1(r) = \frac{F}{2\pi\sqrt{r^2 + 1}}. \quad (4.2)$$

Due to linearity, a summation for multiple sinks is straightforward, so that for the three-dimensional slightly deformed surface, we have

$$\zeta_1(x, y) = \frac{1}{2\pi} \sum_{i=1}^n \frac{F_i}{\sqrt{(x - x'_i)^2 + (y - y'_i)^2 + z_i'^2}}, \quad (4.3)$$

where there are  $n$  sinks, each of dimensionless sink strength  $F_i$  at positions  $(x'_i, y'_i, z'_i)$ .

This small parameter approximation (4.3) will be used for the interface height in the outer region, as well as the initial approximation in the inner region, which is to be iterated on. Using the small parameter approximation for the surface shape in the outer region was shown to be valid in Blake and Kucera [5].

## 4.2 Implementing the integration schemes

As previously mentioned, four applications of the Gauss-Rational rule cannot be used to completely cover the outer region. While this is acceptable when the singularity is away from the boundary between the inner and outer regions, numerical errors increase when the singularity approaches this boundary. As an example, consider  $\int_{-5}^{\infty} \int_5^{\infty} K(x, y) dx dy$  calculated by the Gauss-Rational rule, where  $K$  is the kernel for the first iteration of the coning problem with a single sink,  $F = 1.5$  at  $(0, 0, 1)$ . Table 1 shows results for several placements of the singularity  $(x_0, y_0)$ , comparing the 2D version of the Gauss-Rational rule and 2D DQAGI, the QUADPACK infinite integral routine extended to 2D in the same way as for DQAGS earlier. Tabulated for the 2D Gauss-Rational

Singularity at (0,0)						
2D Gauss-Rational			2D DQAGI			
N	Solution	Diff.	Req.	Solution	Est. Err.	N
4	$6.211991 \times 10^{-5}$		$10^{-4}$	$8.790307 \times 10^{-5}$	$6.7 \times 10^{-5}$	885
16	$8.989224 \times 10^{-5}$	$2.8 \times 10^{-5}$	$10^{-6}$	$8.788414 \times 10^{-5}$	$2.1 \times 10^{-7}$	3735
64	$8.882232 \times 10^{-5}$	$1.7 \times 10^{-6}$	$10^{-8}$	$8.788182 \times 10^{-5}$	$3.8 \times 10^{-9}$	9645
256	$8.788702 \times 10^{-5}$	$3.4 \times 10^{-7}$	$10^{-10}$	$8.788671 \times 10^{-5}$	$1.0 \times 10^{-10}$	40605
1024	$8.788483 \times 10^{-5}$	$2.2 \times 10^{-9}$	$10^{-11}$	$8.788463 \times 10^{-5}$	$9.5 \times 10^{-12}$	107445
Singularity at (4.8,-4.8)						
2D Gauss-Rational			2D DQAGI			
N	Solution	Diff.	Req.	Solution	Est. Err.	N
4	$-2.275674 \times 10^{-6}$		$10^{-4}$	$-4.410515 \times 10^{-6}$	$4.5 \times 10^{-6}$	945
16	$-3.171017 \times 10^{-6}$	$1.4 \times 10^{-6}$	$10^{-6}$	$-4.413032 \times 10^{-6}$	$5.4 \times 10^{-8}$	1635
64	$-4.458318 \times 10^{-6}$	$7.4 \times 10^{-7}$	$10^{-8}$	$-4.412478 \times 10^{-6}$	$3.3 \times 10^{-10}$	8925
256	$-4.414255 \times 10^{-6}$	$4.4 \times 10^{-8}$	$10^{-10}$	$-4.412355 \times 10^{-6}$	$4.5 \times 10^{-11}$	27735
1024	$-4.412495 \times 10^{-6}$	$1.8 \times 10^{-9}$	$10^{-11}$	$-4.412283 \times 10^{-6}$	$9.9 \times 10^{-12}$	46995
Singularity at (4.8,4.8)						
2D Gauss-Rational			2D DQAGI			
N	Solution	Diff.	Req.	Solution	Est. Err.	N
4	$7.451308 \times 10^{-6}$		$10^{-4}$	$-1.585260 \times 10^{-6}$	$1.0 \times 10^{-5}$	1815
16	$4.345856 \times 10^{-5}$	$3.6 \times 10^{-5}$	$10^{-6}$	$3.137626 \times 10^{-6}$	$1.7 \times 10^{-7}$	5985
64	$-1.563571 \times 10^{-6}$	$4.5 \times 10^{-5}$	$10^{-8}$	$3.137574 \times 10^{-6}$	$9.8 \times 10^{-9}$	16035
256	$-1.151385 \times 10^{-6}$	$4.1 \times 10^{-7}$	$10^{-10}$	$3.137698 \times 10^{-6}$	$7.9 \times 10^{-11}$	45405
1024	$6.047972 \times 10^{-6}$	$7.2 \times 10^{-6}$	$10^{-11}$	$3.137761 \times 10^{-6}$	$3.2 \times 10^{-12}$	65085

Table 1: Comparing the 2D Gauss-Rational and 2D DQAGI integration rules for a variety of typical cases for the coning problem.

scheme are the number of function evaluations, the solution, and the difference between successive solutions, and for the 2D DQAGI, the input requested maximum error, the solution, the returned estimated error and the number of function evaluations. When the singularity is at  $(0,0)$ , the Gauss-Rational scheme converges well, as is the case at most other singularity positions in the inner region. Even with the singularity near the corner of the integral region, at  $(4.8, -4.8)$ , the Gauss-Rational scheme performs adequately. However, when the singularity is near a boundary and away from the corner, as at  $(4.8, 4.8)$ , the Gauss-Rational scheme is not converging at all. However, when the Gauss-Rational rule works, it significantly outperforms the 2D form of DQAGI, which requires an excessive number of function evaluations.

To deal with this problem, a buffer zone is introduced. Figure 2 shows how the plane is discretized for integration with the singularity at  $(x_0, y_0)$ . The infinite integrals have been moved away from the boundary of the inner and outer regions, and a buffer region has been introduced. This finite region (triangles 5–12), while near the singularity, can still be efficiently integrated over by Tri-208. Thus, the outer region as shown in Figure 2 is divided into four regions where the Gauss-Rational infinite integration rule is used (numbers 13, 14, 15 and 16) and eight triangles where Tri-208 is applied (numbers 5 to 12). The bounds of the buffer region are  $\pm 2x_{\max}$ ,  $\pm 2y_{\max}$ .

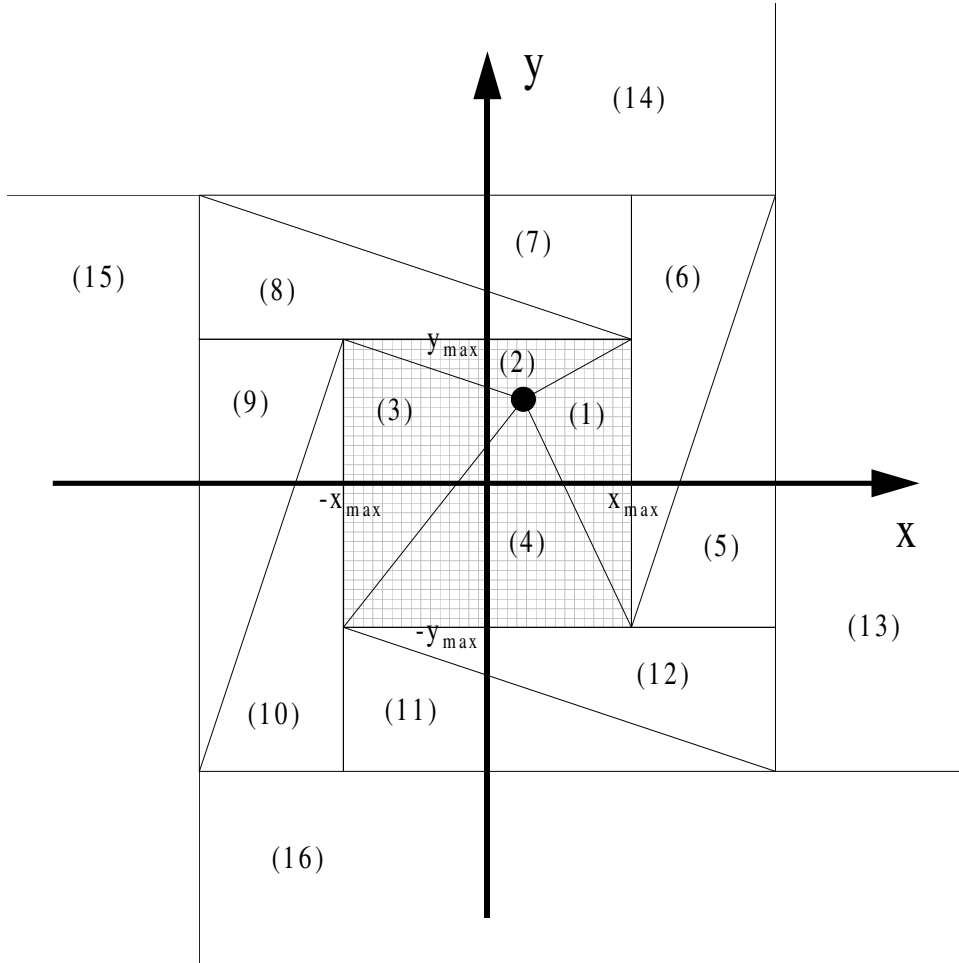


Figure 2: How the region  $\mathcal{R}^2$  is divided up in solving the integral of (3.10) for the singularity at  $(x_0, y_0)$ . The inner region is divided into the triangles 1–4, and the outer region is comprised of the buffer region (triangles 6–12) and the region over which the Gauss Rational scheme is used (triangles 13–16).

Finally, an application of Tri-208 is used on the inner region, where it is divided into four parts (numbers 1, 2, 3 and 4 from Figure 2), each with the singularity at a corner. The region discretization has been formed in such a way that the singularity will always be at a corner of any sub-triangle, so that Tri-208 can eliminate the point singularity, as it has been designed to do.

## 5 Results

Now that we have various of the numerical details in hand, we can solve (3.10) for the steady state interface height given a distribution of oil wells. We note again that this is a steady state problem, leading directly to the interface height after long time. It would be possible to solve for the interface height as an initial value problem, starting was some given  $\zeta$  at time zero, but this would be a substantially harder problem, and is

beyond the scope of this paper.

## 5.1 Further axisymmetric results

The axisymmetric results of Lucas *et al.* [23] are of use in two ways for this more general implementation. The first set of runs of the three-dimensional model were for a single sink at  $(0,0,1)$ , which is identical to the configuration of the axisymmetric problem. Thus, comparisons were made to ensure the correctness of the three-dimensional model. Also, since computation time is large for 3D problems, axisymmetric results were used as a guide to the point density required for the 3D problems.

Some more work on the axisymmetric problem is also briefly included here. Figure 3 is included as a guide to the convergence of the iterative method we have used, comparing the number of iterations required to reach convergence to  $F$ , the dimensionless sink strength parameter, and also includes the curve of  $\zeta(0)$ , the maximum height of the interface as a function of  $F$ . The condition on convergence is that curves from any two successive iterations have a maximum difference between them less than  $10^{-5}$ .

Calculations were also made for the critical pumping rate  $F_c$ , which is the maximum allowable rate of withdrawal that produces a stable cone beneath the well. For  $F > F_c$ , the cone is drawn into the well, and this breakthrough causes unwanted water production. Our method to find  $F_c$  involves testing values of  $F$  until the model breaks down. When the water breakthrough occurs, the interface is no longer smooth, and so the parameter  $c$  from (3.3) is no longer  $1/2$  at the sink. Since  $c = 1/2$  is enforced, numerically this leads to overshoot of the curve over the sink as a solution is attempted iteratively, leading to oscillation of the surface on successive iterations. Thus, a value of  $F$  greater than  $F_c$  is recognized by a surface height greater than one, the dimensionless height of the sink. As is also expected, as  $F$  increases the point density used for calculation of the surface must also be increased, so that results for a particular  $F$  are the same even for higher point densities, to the requested accuracy. Therefore, a valid search for  $F_c$  involves increasing the point density until the values of  $F_c$  converge. For a given point density, a search was done until a value of  $F_c$  could be recognized to three decimal places accuracy, and is shown in Table 2. The number of iterations required, and the height of the interface  $\zeta(r=0)$  for the particular values of  $F$  are also tabulated. Table 2 was produced with points on the range  $[0,10]$ . To check whether this was acceptable, runs were made with the same point densities, but on  $[0,20]$ . The results were the same as those quoted in Table 2. The results for  $F_c$  quoted in Lucas *et al.* [23] are for 100 points on the range 0 to 5, and are hence of less accuracy than those presented here.

## 5.2 Three-dimensional results

The results for three-dimensional problems were initially obtained using QUADPACK integration routines extended to two dimensions, and later using the degenerate quadrilateral adaptive rule. The QUADPACK routines were initially used due to simplicity of implementation, but it was found that the method was quite slow - several hours to days of CPU time on a MIPS R2000 minicomputer were required, particularly when

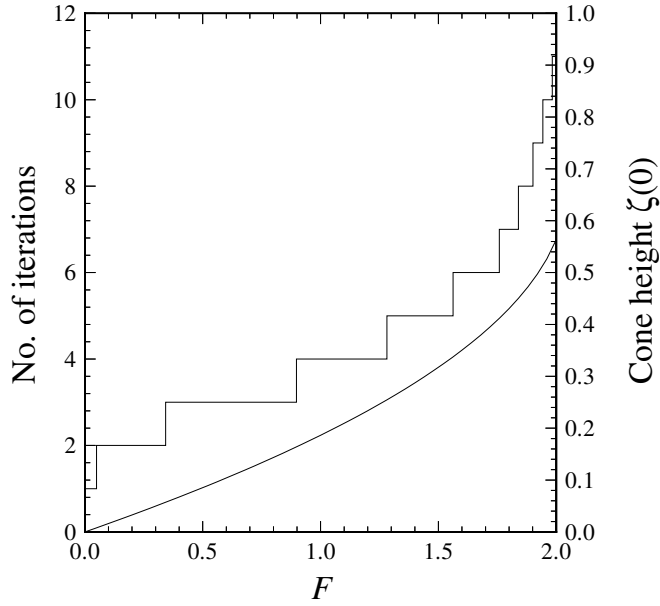


Figure 3: Plot of  $F$  vs Number of iterations for convergence of iterations with a maximum difference of  $5.0 \times 10^{-5}$  for a single sink, and  $F$  vs  $\zeta(0)$  (axisymmetric problem).

No. of points	$F_c$	No. of its.	$\zeta(0)$
10	1.907	71	0.5668
50	2.030	31	0.6255
100	2.043	22	0.6422
500	2.050	24	0.6614
1000	2.050	24	0.6610

Table 2: Critical  $F$  for varying number of points on  $[0, 10]$ .

System	Its.	Time(QUAD)	Time(Tri-208)	$\zeta_{max}$	$\zeta_{max}$ pos.
$F = 1.5$ at $(0, 0, 1)$	4	40900	4480	0.317	$(0,0)$
$F = 1.0$ at $(0, \pm 2, 1)$	3	38800	4220	0.235	$(0,2)$
$F = 1.0$ at $(0, \pm 2, 1)$ $(\pm 2, 0, 1)$	4	133000	12300	0.381	$(0,2)$
$F = 0.5$ at $(0, -2, 1)$ $F = 1.5$ at $(0, 2, 1)$	4	110000	11600	0.349	$(0,2)$

Table 3: Details for selected sink systems. The times are in seconds on a MIPS R2000, rounded to 3 significant figures. The  $\zeta_{max}$  positions are taken in the 1st quadrant when there are duplications.

similar accuracy as was obtained for the axisymmetric problem in [23] was requested. This was the motivation for using the more sophisticated methods. As can be seen from Table 3, where number of iterations to convergence, CPU time for QUADPACK and Tri-208 versions, and maximum interface height and position are tabulated for selected sink systems, the time difference is significant, a factor of about 10. For all following three-dimensional results, we take the size of the inner region to be such that  $x_{\max} = y_{\max} = 5$ .

For the following results, three digits accuracy for the interface solutions was requested. This meant a convergence criterion of maximum difference between successive iterations  $\leq 5.0 \times 10^{-4}$ , and so we chose a maximum error for the adaptive rule for the inner region to be  $1.0 \times 10^{-5}$ , and  $1.0 \times 10^{-6}$  for the outer adaptive buffer zone. In addition, the axisymmetric version was used to find what point density was required for three decimal place accuracy. The accuracy for a particular mesh depends not only on the density of points, but the variation in the surface being found, which depends on the strength of the sinks. It was found that thirty points on  $[0, 5]$  were sufficient up to  $F = 1.5$  (for one sink), and so for all the following 3D results, a  $60 \times 60$  point grid was used on the domain  $-5 \leq x, y \leq 5$ . The only exception was for the single sink  $F = 2.0$ , for which a  $100 \times 100$  point grid was used. Finally, symmetry is used to minimize calculations. If a sink system was symmetric along either of the lines  $x = 0$  or  $y = 0$ , then only one half or one quarter of the node points were used for function and integral evaluations. Table 3 shows the times required for some sink systems, as well as number of iterations to convergence, and the maximum sink heights.

Figure 4 shows a slice through  $x = 0$  for a single sink at  $(0, 0, 1)$  of strengths  $F = 0.5, 1.0, 1.5, 2.0$ . The interface height is identical to that for the axisymmetric formulation of Lucas *et al.* [23] to the order of accuracy requested. In fact, several interface shapes were calculated with a lower error bound than  $10^{-5}$ , and with a corresponding lower convergence criteria. As expected, the computational time required went up considerably for these runs, but further convergence between the axisymmetric and full 3D results was observed. Figure 5 shows contour and surface plots for a single sink at  $(0, 0, 1)$  with strength  $F = 1.5$ . All the surface plots presented here are orthographic, viewed at  $30^\circ$  from the horizontal, with the  $z$ -scale exaggerated by a factor of 20. We note that the slice graph is very smooth since additional points have been added to the output using the bicubic spline interpolation.

There is more interest, of course, in sets of data for three-dimensional problems. Figure 6 shows slices through  $x = 0$  for two sinks, both with  $F = 1.0$ , at positions  $(0, \pm y, 1)$ ,  $y = 0.5, 1.0, 1.5, 2.0, 2.5$ . We can see the way the two sinks interact, giving a more raised interface height as the sinks move closer together. It should be noted that the interface height is not simply the sum of interface heights for two separate curves, but a more complicated nonlinear combination. Also, the highest point of the surface is not always directly under a sink. For  $y = 0.5, 1.0$  in the set shown here, the highest points are between the sinks. Figure 7 shows contour and surface plots for the case of two sinks of strength  $F = 1.0$  at  $(0, \pm 2, 1)$ . Figure 8 is also included to indicate the speed of convergence of the iterative method used here. It shows the interface height at each iteration for two of the two-sink cases. Convergence is quite rapid, and in both cases plotted the last two iterations are indistinguishable.

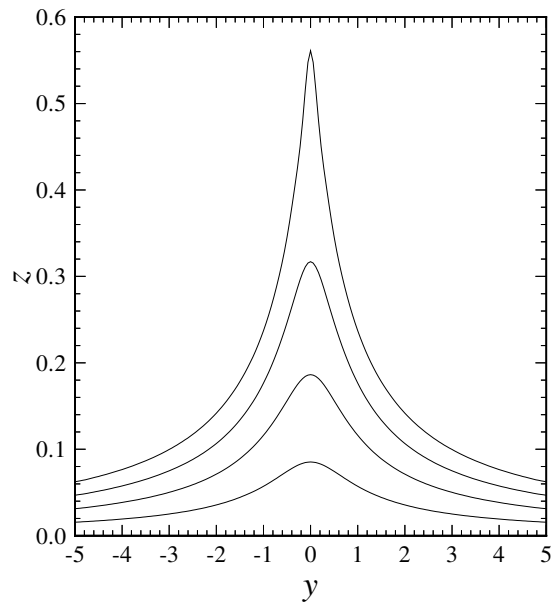


Figure 4: Interface shape through  $x = 0$ , 1 sink,  $F = 0.5$  (lowest curve), 1.0, 1.5, 2.0 (highest curve) at  $(0, 0, 1)$ .

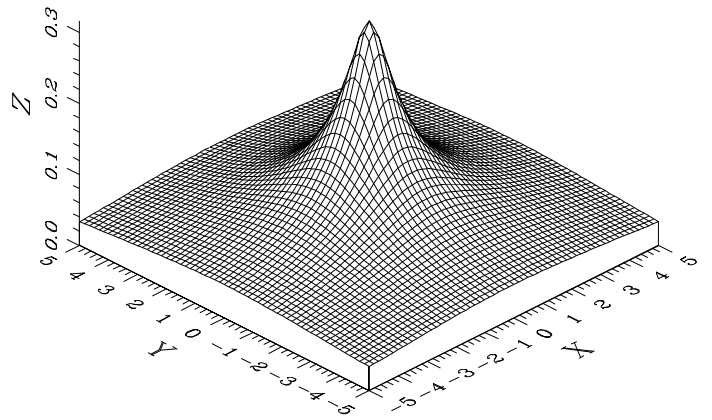
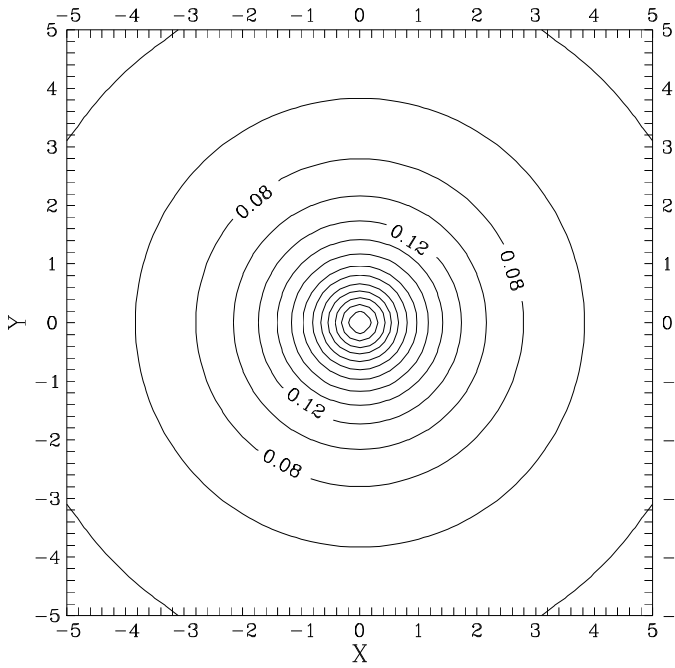


Figure 5: Interface shape for 1 sink,  $F = 1.5$  at  $(0, 0, 1)$ , contour and surface plots.

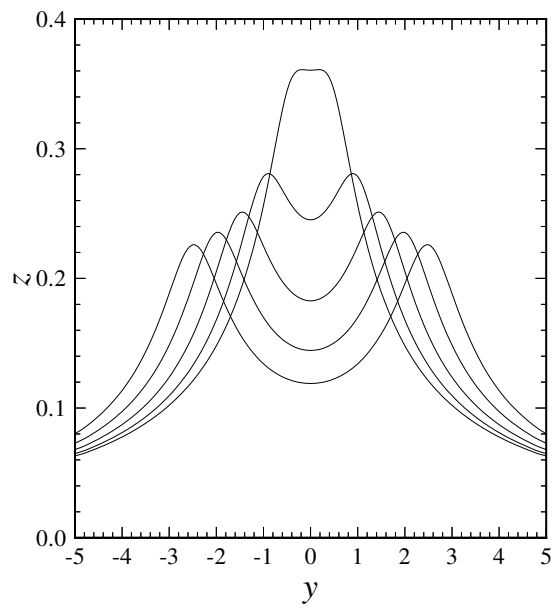


Figure 6: Interface shape through  $x = 0$ , 2 sinks,  $F = 1.0$  at  $(0, \pm y, 1)$ , where  $y = 0.5$  (highest curve), 1.0, 1.5, 2.0, 2.5 (lowest curve).

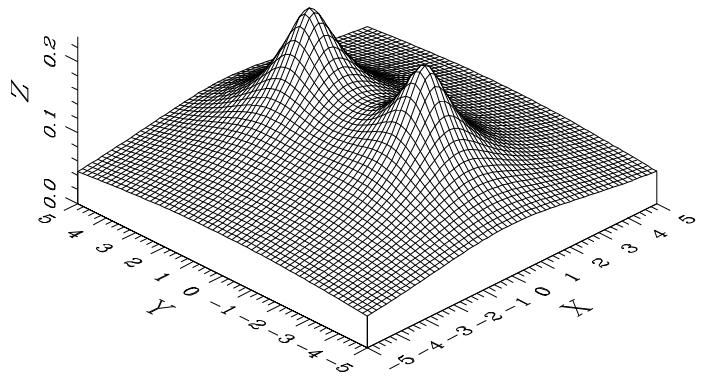
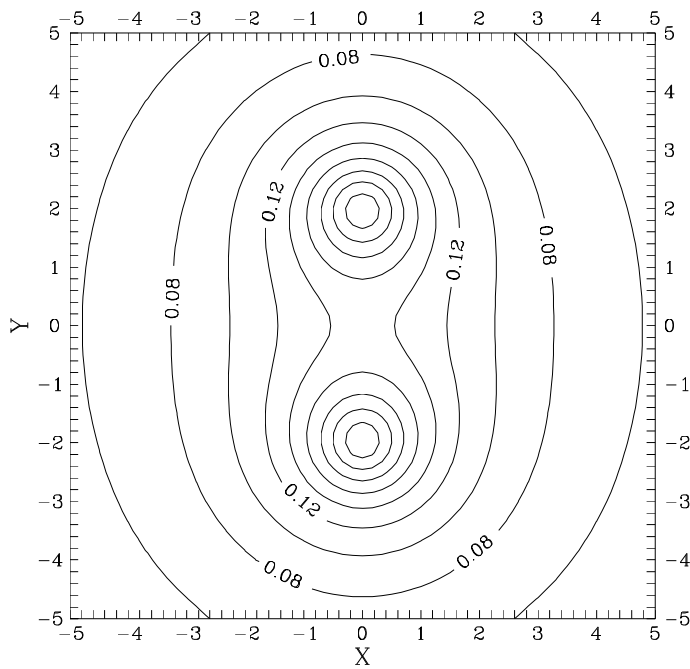


Figure 7: Interface shape for 2 sinks,  $F = 1.0$  at  $(0, \pm 2, 1)$ , contour and surface plots.

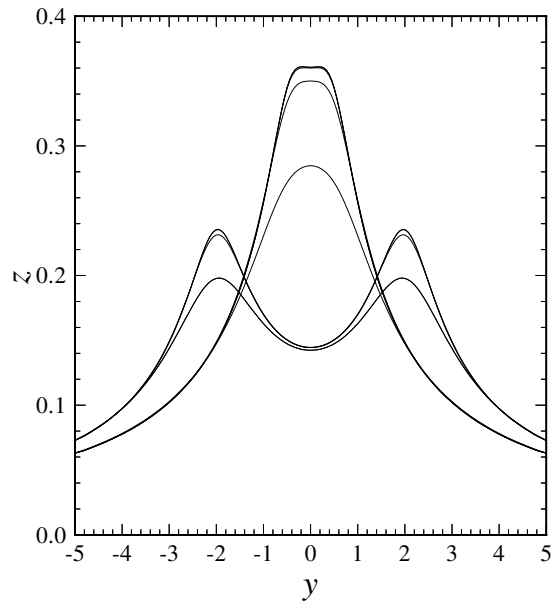


Figure 8: Interface shape through  $x = 0$ , each of 3 iterations for 2 sinks,  $F = 1.0$  at  $(0, \pm 2, 1)$ , and 4 iterations for 2 sinks,  $F = 1.0$  at  $(0, \pm 0.5, 1)$ . The “0th” iteration (initial approximation) is also included.

---

Figure 9 shows slices through  $x = 0$  for two sinks, one at  $(0, -2, 1)$  with  $F = 1.5$  and the other at  $(0, 2, 1)$  with  $F = 0.0, 0.5, 1.0, 1.5$ . This result shows the effect of the interface near one sink as the other sink’s strength varies. Figure 10 shows contour and surface plots for  $F = 0.5$  at  $(0, -2, 1)$  and  $F = 1.5$  at  $(0, 2, 1)$ . Figure 11 shows a slice through  $x = 0$  and Figure 12 shows contour and surface plots for the case of four sinks, each of strength  $F = 1.0$ , at  $(0, \pm 2, 1), (\pm 2, 0, 1)$ . These results should be compared with the results of Figure 6 for just two sinks at the same distance, and shows quite well the effect of multiple oil wells operating close together.

Finally, as an indication of the general nature of the formulation described here, Figure 13 was produced, showing the interface shape for a random setup of sinks representing oil wells. Disordered sink configurations, such as in Figure 13 are dealt with just as easily; just four iterations were required to obtain the steady state interface shape for this sink configuration.

## 6 Conclusion

We have developed a boundary integral method which determines the steady state height of the interface between oil and water in an oil reservoir under the influence of a distribution of oil wells pumping oil to the surface. We are able to find an interface shape for any general sink distribution, as opposed to the limited case of [23], where only axisymmetric problems could be handled. However, Table 3 shows that the CPU time required for a three-dimensional problem is significantly larger than for axisymmetric problems.

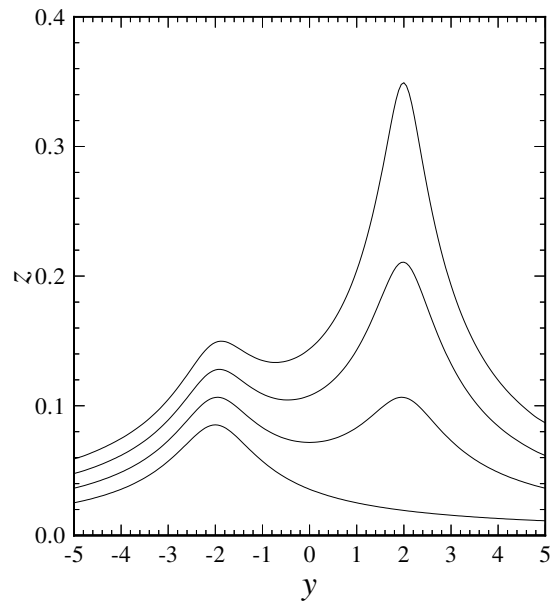


Figure 9: Interface shape through  $x = 0$ , 2 sinks,  $F = 0.5$  at  $(0, -2, 1)$ ,  $F = 0.0$  (lowest curve), 0.5, 1.0, 1.5 (highest curve) at  $(0, 2, 1)$ .

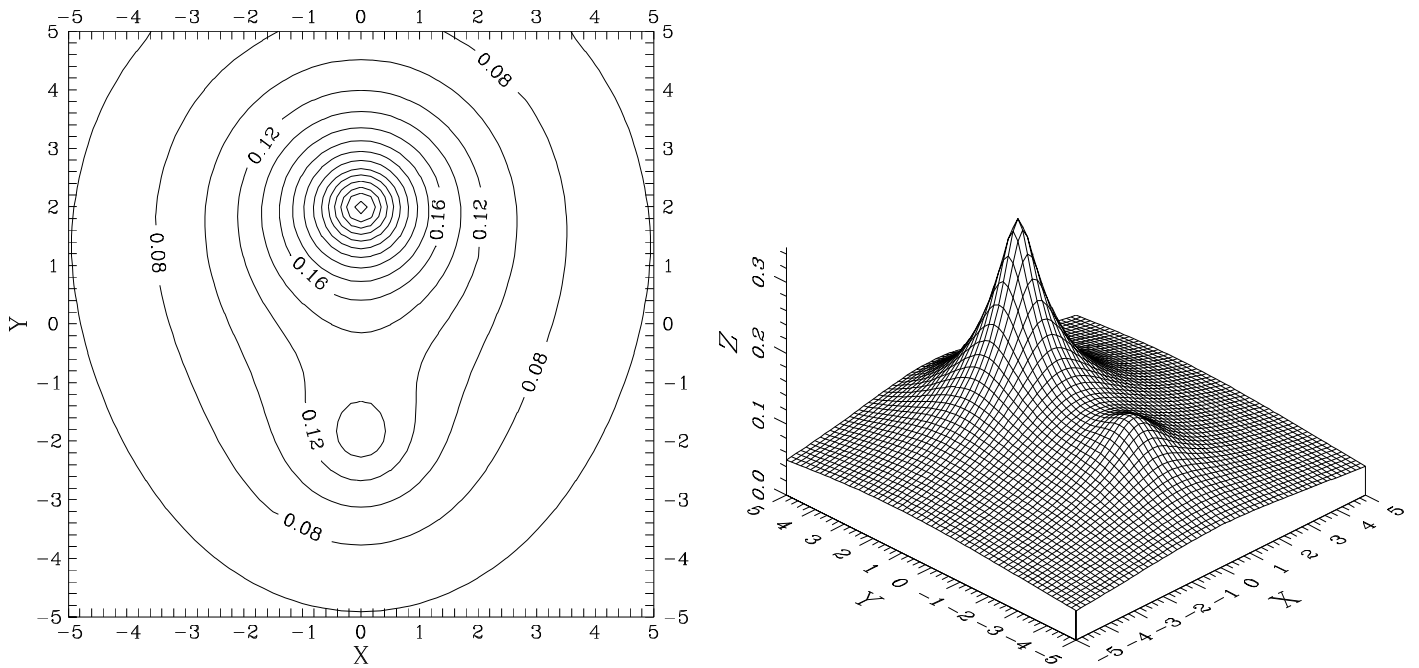


Figure 10: Interface for 2 sinks,  $F = 0.5$  at  $(0, -2, 1)$ ,  $F = 1.0$  at  $(0, 2, 1)$ , contour and surface plots.

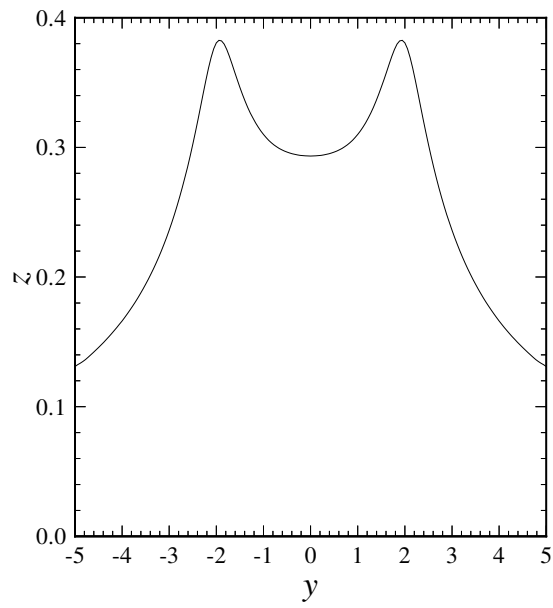


Figure 11: Interface shape through  $x = 0$ , 4 sinks,  $F = 1.0$  at  $(0, \pm 2, 1)$ ,  $(\pm 2, 0, 1)$ .

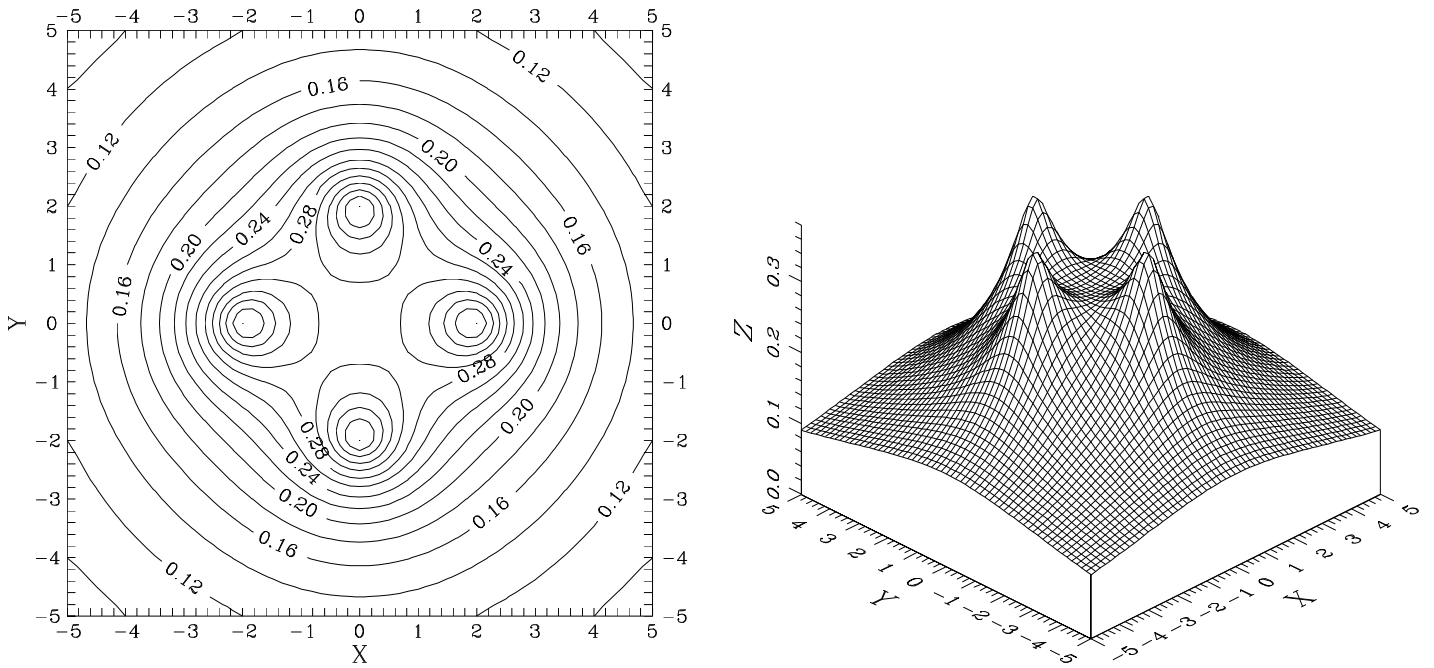


Figure 12: Interface shape for 4 sinks,  $F = 1.0$  at  $(0, \pm 2, 1)$ ,  $(\pm 2, 0, 1)$ , contour and surface plots.

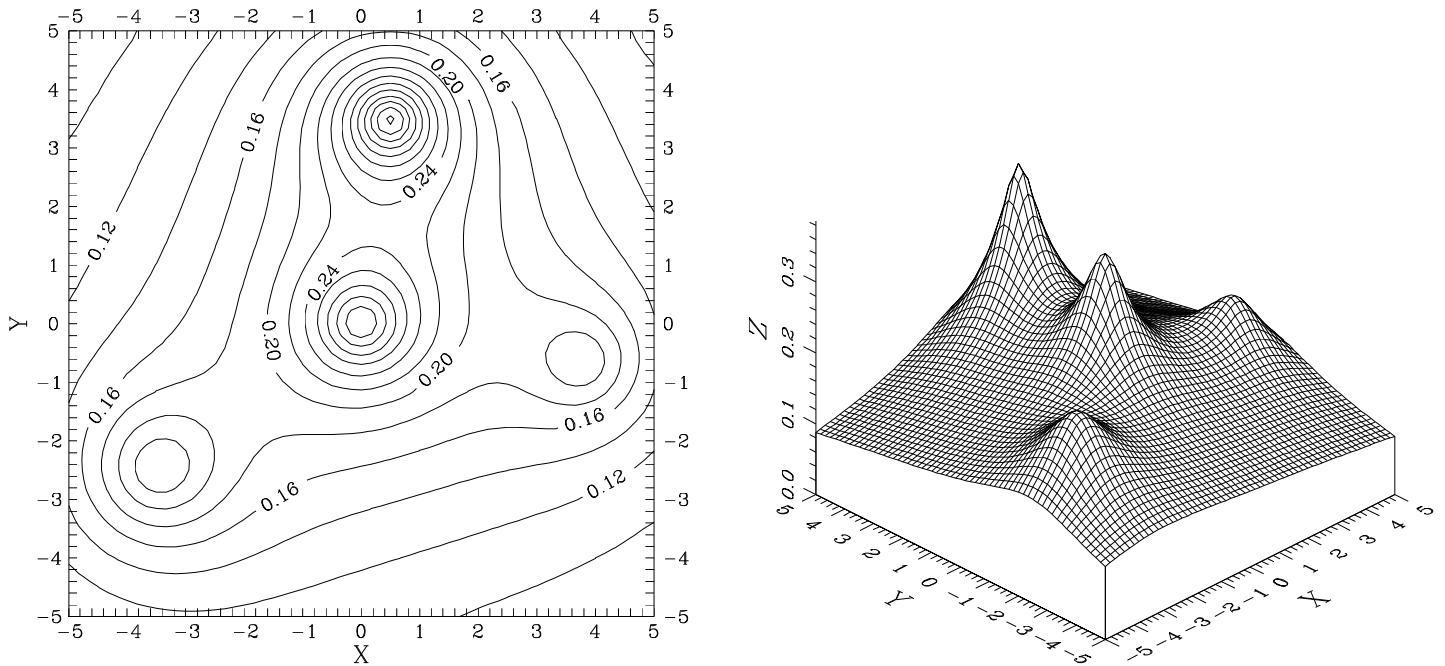


Figure 13: Contour and surface plots for 4 sinks,  $F = 1$  at  $(-3\frac{1}{2}, -2\frac{1}{2}, 1\frac{1}{5})$ ,  $F = 1$  at  $(0, 0, 1)$ ,  $F = 1\frac{3}{10}$  at  $(\frac{1}{2}, 3\frac{1}{2}, 1)$ , and  $F = \frac{3}{5}$  at  $(3\frac{5}{6}, -\frac{2}{3}, 1)$ .

As an example, a slowly converging axisymmetric problem (100 points,  $F = 2.0$ , 11 iterations required) took only 114 seconds on the MIPS R2000. Breakthrough values of  $F$  can in principle be calculated, but such critical values  $F_c$  depend on particular sink distributions, and it is not obvious how to develop general rules.

Various methods have been investigated for evaluating the difficult two-dimensional integrals involved in the three-dimensional coning problem. We have seen how the 1D QUADPACK routines expanded to two dimensions perform well, but that their error estimates are wildly pessimistic, leading to an excessive number of integrand evaluations. The IMT rule, while conceptually quite elegant, failed to be of any real practical use when extended to two dimensions and applied to the coning integrand using a compiler limited to double precision. The overall advantage of the degenerate quadrilateral approach in dealing with point singularities, coupled with the described adaptive algorithm can be easily seen. Not only does this method have good convergence properties, but the error estimates are also good measures, especially compared to DQAGS.

We once again emphasize the simplifications used to obtain this model. This is a steady state model, giving the interface shape arrived at after a long time. The rock strata is assumed to be of infinite extent, and be a homogeneous medium of constant permeability  $k$ . The fact that vertical permeability is often 1/10 to 1/100 of horizontal permeability can be resolved by stretching the vertical coordinates. The major drawback with this model is that oil bearing rock is rarely homogeneous. Detailed knowledge of the rock's characteristics would be needed for more accurate interface shapes, which is rarely feasible in practical situations.

There are a number of potentially useful extensions of this work. Here, oil wells have been modelled by point sinks and assumed the reservoir is of infinite extent. More

realistic models for the oil well could be used, such as line sinks. While the results of Lucas *et al.* [23] do not show dramatically different results for line as opposed to point sinks in the axisymmetric case, angled line sinks could be of interest. Finally, impermeable layers could be introduced to model the finite size of an oil reservoir. In some cases this may lead to no stable cone shape, as in Bruining *et al.* [7], and in these cases, a time-dependent model would be required to model the evolution of the oil-water interface.

### **Acknowledgments**

This work forms part of the Ph.D. thesis of S.K.L., written under the supervision Professor N. Phan-Thien at the Department of Mechanical and Mechatronic Engineering, University of Sydney, and was supported in part by an ARC grant. S.K.L. wishes to thank Professor H. A. Stone for editorial advice concerning the final form of this paper.

# Appendix A Integration Rules

This Appendix contains details on the various integration routines used in solving the three-dimensional coning problem.

## A.1 The Gauss-Rational scheme

Quite often infinite integrals, have a long “tail”, in that  $f(x) \rightarrow 0$  slowly as  $x \rightarrow \infty$ . For such integrals, quadrature rules such as the Gauss-Laguerre rule are inappropriate. Here, we outline the Gauss-Rational rule, which is more appropriate for long-tailed integrals, as developed in Delves and Mohamed [10].

Consider the integral

$$I = \int_a^\infty f(s) ds. \quad (\text{A.1})$$

Let  $s = 2(a + \alpha)/(s' + 1) - \alpha$ , where  $\alpha$  is arbitrary, but constrained by  $a + \alpha > 0$ . Then (A.1) becomes

$$I = 2(a + \alpha) \int_{-1}^1 \frac{F(s')}{(s' + 1)^2} ds', \quad \text{where } F(s') = f(s). \quad (\text{A.2})$$

Taking  $\{\xi_i, w_i, i = 1, \dots, N\}$  as points and weights for the  $N$ -point Gauss-Legendre rule, then the approximation

$$I \approx I_N = 2(a + \alpha) \sum_{i=1}^N w_i \frac{F(\xi_i)}{(\xi_i + 1)^2}, \quad (\text{A.3})$$

will be an identity if  $F(s')/(s' + 1)^2$  is a polynomial of degree  $\leq 2N - 1$  in  $s'$ , i.e., if  $F(s') = (s' + 1)^k$ ,  $k = 2, 3, \dots, 2N + 1$  is its annihilation class. This leads to the rule

$$\int_a^\infty f(s) ds \approx \sum_{i=1}^N w'_i f(\xi'_i), \quad \text{where } \xi'_i = \frac{2(a + \alpha)}{(\xi_i + 1)} - \alpha, \quad w'_i = \frac{2(a + \alpha)w_i}{(\xi_i + 1)^2}, \quad (\text{A.4})$$

where  $\xi_i, w_i$  are Gauss-Legendre points and weights, which, due to its annihilation class, is better suited to long-tailed integrals than for example a Gauss-Laguerre rule with its exponentially decaying weight function. Equation (A.4) is known as a Gauss-Rational rule, where the arbitrary value  $\alpha$  is a measure of the spread of the node points from  $[-1, 1]$  to  $[a, \infty]$ , and has some optimal value for any particular integral.

A two-dimensional form of the Gauss-Rational rule is easily described as

$$\int_b^\infty \int_a^\infty f(x, y) dx dy = \sum_{i=1}^N \sum_{j=1}^M w_{1i} w_{2j} f(\xi_{1i}, \xi_{2j}), \quad (\text{A.5})$$

where

$$\left. \begin{aligned} \xi_{1i} &= \frac{2(a + \alpha_1)}{(\xi_i + 1)} - \alpha_1, & w_{1i} &= \frac{2(a + \alpha_1)w_i}{(\xi_i + 1)^2}, & \text{for } \alpha_1 > -a, \\ \xi_{2j} &= \frac{2(a + \alpha_2)}{(\xi_j + 1)} - \alpha_2, & w_{2j} &= \frac{2(a + \alpha_2)w_j}{(\xi_j + 1)^2}, & \text{for } \alpha_2 > -b. \end{aligned} \right\} \quad (\text{A.6})$$

Tests using this quadrature rule on integrals that are required in the outer region for the coning problem have shown that setting  $a + \alpha_1 = 5$ ,  $b + \alpha_2 = 5$ , and  $N = M = 16$  gives acceptable accuracy, as long as the singularity is kept away from the boundary of the region being integrated over. The quadrature rule (A.5) can be used to cover the entire outer region for the coning problem using appropriate substitutions.

## A.2 The IMT rule

The IMT rule is a 1D quadrature rule developed by Iri, Moriguti and Takasawa [16], and is a general transformation technique for eliminating end point singularities, regardless of type. We include here an outline to the method, and its application to the coning problem, since the method is potentially useful though appears not well known in the fluid dynamics literature.

Set

$$Q = \int_0^1 e^{-(1/t)-(1/(1-t))} dt = 0.00702\,98584 \dots, \quad (\text{A.7})$$

and define  $\phi(t)$  by

$$\phi(t) = \int_0^t \phi'(\tau) d\tau, \quad \phi'(t) = \frac{1}{Q} e^{-(1/t)-(1/(1-t))}. \quad (\text{A.8})$$

Then, using the transform  $x = \phi(t)$ ,

$$\int_0^1 f(x) dx = \int_0^1 f(\phi(t))\phi'(t) dt = \int_0^1 g(t) dt. \quad (\text{A.9})$$

If  $f(x)$  is differentiable infinitely many times on  $(0,1)$  and is continuous or has an algebraic singularity at the end points, then  $g(t)$  will be differentiable infinitely many times on  $[0,1]$ , and all its derivatives at end points, as well as  $g$  itself, will vanish at the end points, i.e.,  $g^{(m)}(0) = g^{(m)}(1) = 0$ , for  $m = 0, 1, 2, \dots$ . But, the integral of  $g$  is of the form where the error when using the Euler-Maclaurin integration formula decreases exponentially. Thus, a quadrature rule to obtain high accuracy for integrals with end point singularities, known as the IMT rule after its authors, is

$$\int_0^1 f(x) dx \approx \frac{1}{N} \sum_{n=1}^{N-1} w_n^{(N)} f\left(x_n^{(N)}\right), \quad \text{where } x_n^{(N)} = \phi\left(\frac{n}{N}\right), \quad w_n^{(N)} = \phi'\left(\frac{n}{N}\right). \quad (\text{A.10})$$

The points and weights for this method are listed for  $N$  as powers of two in Iri *et al.* [16], and transforming the integration interval from  $[0, 1]$  to  $[a, b]$ , as well as forming a two-dimensional form, are straightforward.

Figure 14 compares evaluating

$$\int_0^1 x^{-1/2} dx \quad (= 2), \quad (\text{A.11})$$

using the IMT rule, the QUADPACK routines DQAG and DQAGS, which are adaptive routines, the second using extrapolation, and Gauss-Legendre and Gauss-Chebyshev quadrature. The exponential decay of the IMT rule error can be seen, as well as its

superiority over the other methods. Only the extrapolation of DQAGS came close, but gave nothing between poor and machine accuracy results for this simple integrand. It was also found that, when the upper end point of (A.11) was changed from one to successively smaller values (also changing the solution), the relative error for the IMT rule was found to be the same, while it increases when DQAG is used. This indicates that making a smaller region around a singularity for integration will not improve the convergence of an adaptive method, but can improve the performance of the IMT rule.

The 2D version of the IMT rule was also tested on the kernel of the integral in (3.10), using a single sink with  $F = 2.0$  at  $(0, 0, 1)$ , the small parameter approximation for  $\zeta$ ,  $\partial\zeta/\partial x$ , and  $\partial\zeta/\partial y$ , setting  $x_0 = y_0 = 0$ , and integrating over  $\int_0^a \int_0^a K(x, y) dx dy$ , with  $a = 0.25$  and  $5$ . The solutions for these two cases are  $-1.653039238 \times 10^{-3}$  and  $-2.8652616094 \times 10^{-3}$  respectively. Figure 15 plots  $N$  versus relative error for the 2D IMT rule and 2D DQAGS implementations, as well as the DQAGS estimated error, returned from the routine. The 2D DQAGS rule is a duplication of DQAGS, with the error estimate defined in Piessens *et al.* [26] for a two-dimensional implementation being returned. Reducing the size of the region has an effect on the 2D DQAGS error, although it is not as consistent as for the IMT rule. What is of importance, however, is the difference between the estimated and actual errors for the 2D DQAGS rule. The difference is of several orders of magnitude, which leads to an excessive number of evaluations given a requested error.

One final point must be made about the IMT rule. As  $N$  increases, quadrature points become increasingly close to the end points. For example, for  $N = 64$ , there is a quadrature point at  $1.957 \times 10^{-30}$  on  $[0, 1]$ . When the rule is transformed to  $[a, b]$ , this will be lost in double precision FORTRAN if  $a \sim O(1)$ , leading to round-off errors. Even with  $N = 32$ , a point is at  $5.913 \times 10^{-16}$ , which when added to  $a$  can lead to significant round-off error when the singularity is at  $a$ . For this reason, the limit of  $N = 16$  is required, and so the  $15 \times 15$  point IMT rule for integrating over a rectangular region with a singularity at a corner is used. As will see later, even this rule can lead to round-off error. For small regions, the  $15 \times 15$  rule has round-off error for the coning problem's kernel when using double precision arithmetic. This is why the integration error curves using the IMT rule in Figure 17 do not continue to smaller error levels.

### A.3 Degenerate quadrilaterals

Consider integrating over a triangle an integrand which is singular at one corner; for example,

$$I = \int_0^1 \int_0^x \frac{1}{\sqrt{x^2 + y^2}} dy dx. \quad (\text{A.12})$$

Using the transform  $u = x$  and  $v = y/x$ , the Jacobian is  $J = u$ , and (A.12) becomes

$$I = \int_0^1 \int_0^1 \frac{1}{\sqrt{1 + v^2}} dv du \quad (= \ln(1 + \sqrt{2})). \quad (\text{A.13})$$

By “stretching” the singular point into a line, the integral in  $(u, v)$  space is no longer singular. Thus, a useful technique for integrals involving point singularities is to take

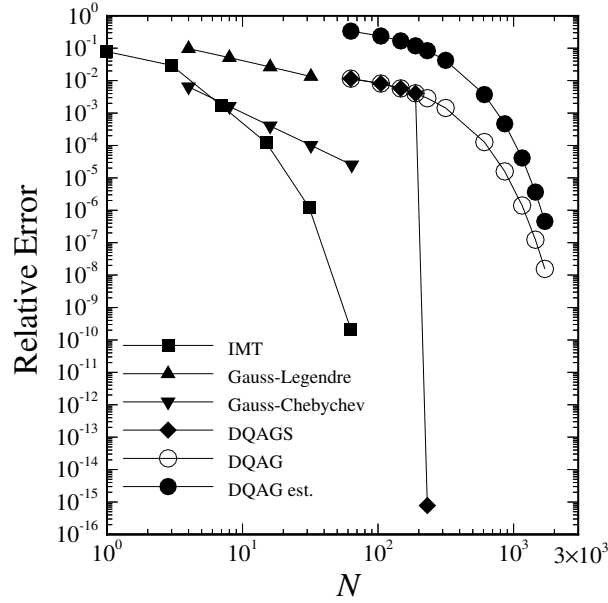


Figure 14: Relative error versus Number of function evaluations for evaluating  $\int_0^1 x^{-1/2} dx$ , comparing the IMT, Gauss-Legendre, Gauss-Chebyshev, and QUADPACK DQAG and DQAGS routines. The upper curve for DQAG is the returned estimate of error.

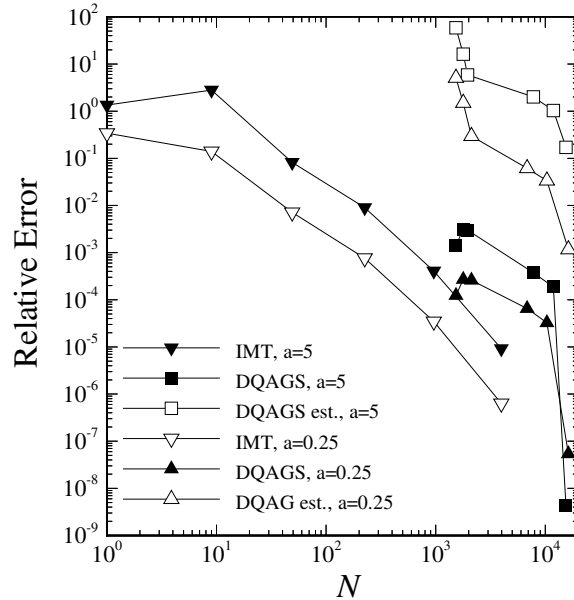


Figure 15: Relative error versus Number of function evaluations for the 2D IMT and 2D DQAGS rules, and estimated error for 2D DQAGS, for  $\int_0^a \int_0^a K(x, y) dx dy$ , where  $K$  is the kernel for  $F = 2.0$  at  $(0, 0, 1)$ ,  $(x_0, y_0) = (0, 0)$ , and  $a = 5, 0.25$ .

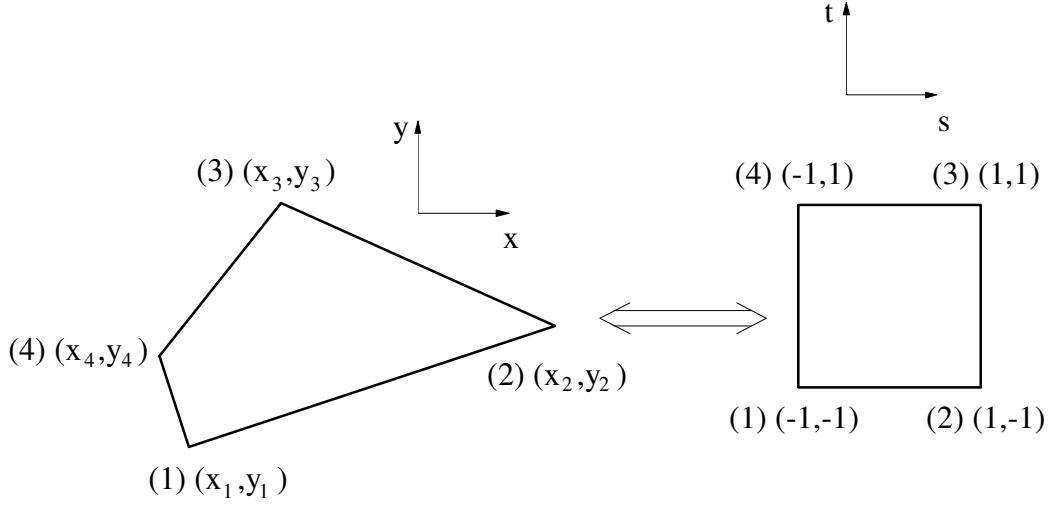


Figure 16: The transformation between world and normalized coordinates for a general quadrilateral.

a quadrature rule based on a general quadrilateral, and use it with two of its corners being identical; the quadrilateral has become degenerate – a triangle.

Consider the transform  $(x, y) \iff (s, t)$  as shown in Figure 16. If we let

$$\left. \begin{aligned} \phi_1(s, t) &= (1-s)(1-t)/4, & \phi_2(s, t) &= (1+s)(1-t)/4, \\ \phi_3(s, t) &= (1+s)(1+t)/4, & \phi_4(s, t) &= (1-s)(1+t)/4, \end{aligned} \right\} \quad (\text{A.14})$$

then the appropriate transform is

$$x = \sum_{i=1}^4 \phi_i x_i, \quad y = \sum_{i=1}^4 \phi_i y_i, \quad (\text{A.15})$$

where  $(x_i, y_i), i = 1, \dots, 4$  are the coordinates of the corners of the general quadrilateral. Using the standard 2D transformation rule for integration, we can get, using an  $N \times N$  point Gauss-Legendre rule on  $[-1, 1] \times [-1, 1]$  in  $(s, t)$  space, the quadrature rule for a quadrilateral

$$\iint_{R_{xy}} f(x, y) dx dy \simeq \sum_{i=1}^N \sum_{j=1}^N f(\eta_{ij}, \nu_{ij}) |J_{ij}| w_{ij}, \quad (\text{A.16})$$

where

$$\eta_{ij} = \sum_{k=1}^4 \phi_k(\xi_i, \xi_j) x_k, \quad \nu_{ij} = \sum_{k=1}^4 \phi_k(\xi_i, \xi_j) y_k, \quad (\text{A.17})$$

$$J_{ij} = \left. \frac{\partial x}{\partial s} \frac{\partial y}{\partial t} - \frac{\partial x}{\partial t} \frac{\partial y}{\partial s} \right|_{s=\xi_i, t=\xi_j}, \quad (\text{A.18})$$

$$\left. \begin{aligned} \frac{\partial x}{\partial s} &= (x_1 - x_2 + x_3 - x_4)t/4 + (-x_1 + x_2 + x_3 - x_4)/4, \\ \frac{\partial y}{\partial s} &= (y_1 - y_2 + y_3 - y_4)t/4 + (-y_1 + y_2 + y_3 - y_4)/4, \\ \frac{\partial x}{\partial t} &= (x_1 - x_2 + x_3 - x_4)s/4 + (-x_1 - x_2 + x_3 + x_4)/4, \\ \frac{\partial y}{\partial t} &= (y_1 - y_2 + y_3 - y_4)s/4 + (-y_1 - y_2 + y_3 + y_4)/4, \end{aligned} \right\} \quad (\text{A.19})$$

and the  $(\xi_i, w_i)$  are the points and weights for an N-point Gauss-Legendre quadrature. If two of the corners  $(x_i, y_i)$  are the same, the quadrilateral degenerates into a triangle, and this transform eliminates a  $1/r$  type singularity at the degenerate corner of the triangle.

The degenerate quadrilateral technique for eliminating point singularities has an interesting history. Lachat and Watson [19] first used degenerate elements in a similar manner to this in an early boundary integral formulation, and some researchers since (for example, Amini and Harris [1] and Lean and Wexler [20]) have used this technique in the boundary element literature. Degenerate quadrilaterals are also known as Duffy's triangles, in the literature that cites Duffy [11]. While also considering three-dimensional volume integrals with a point singularity, the formulation of Duffy is identical to that of Lachat and Watson. In fact, the degenerate quadrilateral technique continues to be rediscovered, for example in Li *et al.* [21]. Rizzo and Shippy [28] used a similar method based on a transform to polar coordinates to eliminate the singularity. This method, however, leads to complicated integral boundaries involving inverse trigonometric functions when dealing with integrals over rectangular or triangular regions, due to the transform of the sector of a circle to a square.

The degenerate quadrilateral method can also be used to integrate over triangles with no singularities, so that the same rule can be used for other two-dimensional integrals. Investigation has shown that placing the degeneracy at the point with the largest angle of the triangle leads to the smallest error, a reasonable result since it ensures the maximum spread of the quadrature points that are concentrated near the degenerate point.

## A.4 Adaptive 2D numerical integrators

Since other methods are used to deal with the singularity in the integral of (3.10), integration over the inner region does not require the complicated extrapolation of DQAGS (Piessens *et al.* [26]). The simpler adaptive routine DQAG is more appropriate. However, it would be preferable to have an explicitly two-dimensional formulation. To this end, a 2D analog of DQAG was developed, based on the work of Kahaner and Rechar [17], which has the algorithm:

Input the region (as a set of rectangles or triangles) and the requested error.

Initialize the result as an approximation over the entire region.

While the estimate of total error  $>$  requested error,

Subdivide the region with the largest error into 2 equal sub-regions.

Calculate approximations over each sub-region.

Update the result and total error.

Several different adaptive 2D integration algorithms were implemented and tested for the coning problem. Initially, rectangular regions were tried, using a  $15 \times 15$  point 2D Kronrod rule. A  $2N + 1$  point Kronrod rule has an  $N$  point Gauss-Legendre quadrature points embedded within it for the purposes of error estimation. However, due to the singularity in the problem, an algorithm based on the  $15 \times 15$  point IMT rule was also implemented. Since the IMT rule is based upon the trapezoidal rule, it has the  $7 \times 7$  point rule embedded in it, again for use as an error estimate. Rectangles were split by bisecting their longest sides. Code were also developed based on triangles, where Gauss-Legendre rules are used on degenerate quadrilaterals. If there is a singularity at a corner, the degeneracy is placed at that point, else it is placed at the corner with the largest angle. Here two sets of rules were used; first  $4 \times 4$  and  $6 \times 6$  Gauss-Legendre rules totaling 52 quadrature points, and then  $8 \times 8$  and  $12 \times 12$  rules using 208 points. The higher order rule is used to give the integral estimate, while the difference between the two rules gives the error estimate. Triangles were subdivided by a line joining the midpoint of the longest side to the triangle's opposite corner.

As in Kahaner and Rechar [17], data on points defining the region, and approximations of the region's integral and error, are kept in a heap, so that the region with the largest current error is referenced as the top node of the heap, and removal and addition of elements to a heap while retaining its order is a simple operation. The heap sort is in fact ideal for this type of problem (see Knuth [18]). The idea from [17] of initially passing to an adaptive routine more than one region is also implemented. By using this method, the one error estimate can be requested for more complicated regions made up of several rectangles or triangles. This is especially useful for the coning problem, where the singularity must be put at a corner within the integration region.

Figures 17 and 18 are a guide to the efficiency of the various schemes for solving complex 2D integration problems. The integral  $\int_0^5 \int_0^5 K(x, y) dx dy$  is evaluated, where  $K(x, y)$  is the integrand of (3.10), the sink system is two sinks,  $F = 0.5$  at  $(0, -2, 1)$  and  $F = 1.5$  at  $(0, 2, 1)$ ,  $(x_0, y_0) = (0, 0)$ , and the surface and its derivatives are represented by the first order small parameter solution of Section 4.1. In the legend of the figures, Tri-52 and Tri-208 are 2D adaptive rules using degenerate quadrilaterals and 52 and 208 quadrature points respectively, 2DQAGS is the extrapolative QUADPACK routine extended to two dimensions, and Kronrod and IMT are 2D adaptive rules on rectangles using the fifteen point Kronrod rule and fifteen point IMT rule respectively. Figure 17 compares  $N$ , the number of function evaluations, to the relative error, while Figure 18 compares  $N$  with the estimated relative error returned from the various routines. The exact value, by convergence of the various methods, is  $-6.48045122811 \times 10^{-4}$ .

There are several points to note from these results. The better performance of the degenerate quadrilateral method compared to the others, based on both actual and estimated error, is immediately obvious. The poor performance and short range of the method based on the IMT rule is a little surprising considering its good 1D performance. Finally, note how poorly the 2D version of DQAGS performs. While its actual error convergence is comparable to Tri-208, although with roughly an order of magnitude more function evaluations, its estimated error performance is quite bad. Solutions to the coning problem using QUADPACK will be much more accurate for a given required

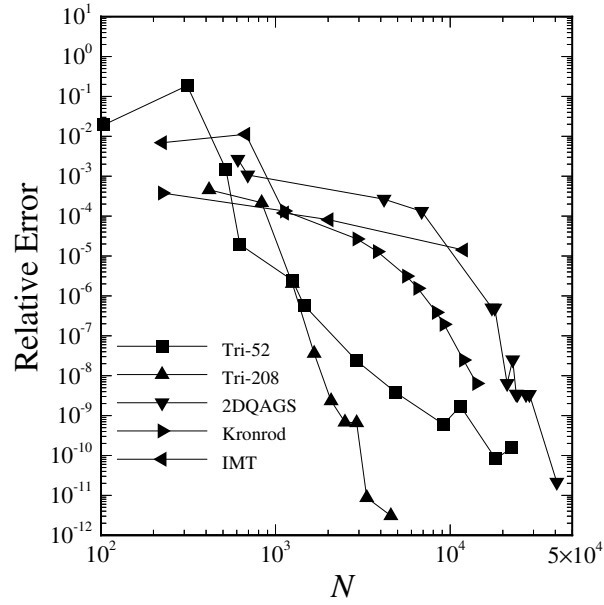


Figure 17: Relative error versus Number of function evaluations for the variety of two-dimensional integration routines listed in the text.

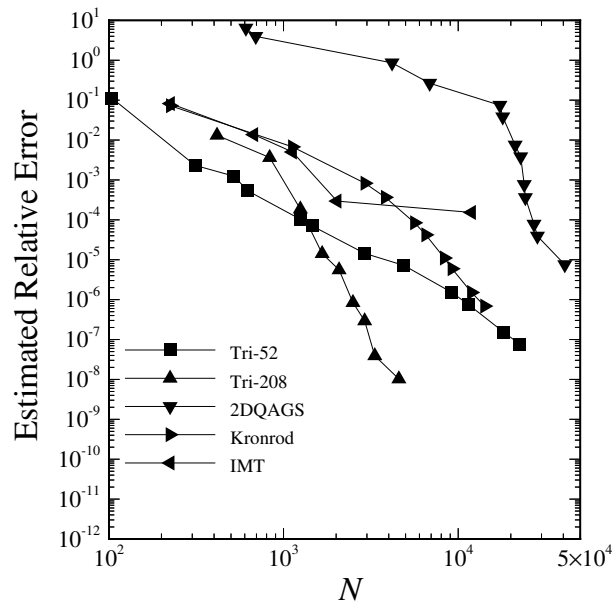


Figure 18: Estimated relative error returned versus Number of function evaluations for the variety of two-dimensional integration routines listed in the text.

error, but will also require far more function evaluations than other methods. As a result of these comparisons, the adaptive algorithm on triangular regions, using the degenerate quadrilateral mapping, Tri-208, is used in evaluating the integrals in (3.10).

## References

- [1] S. Amini and P.J. Harris, A comparison between various boundary integral formulations for the exterior acoustic problem, *Comput. Methods Appl. Mech. Eng.*, **84** (1990), 59–75.
- [2] J. Bear, *Dynamics of Fluids in Porous Media*, (McGraw-Hill, New York, 1972).
- [3] J. Bear and G. Dagan, Some exact solutions of interface problems by means of the hodograph method, *J. Geophys. Res.*, **69** (1964), 1563–1572
- [4] D.E. Beskos (ed), *Boundary Element Methods in Mechanics*, (North-Holland, Amsterdam, 1987).
- [5] J.R. Blake and A. Kucera, Coning in oil reservoirs, *Math. Scientist*, **13** (1988), 36–47.
- [6] C.A. Brebbia, J.C.F. Telles, and L.C. Wrobel, *Boundary Element Techniques*, (Springer-Verlag, Berlin, 1984).
- [7] J. Bruining, C.J. Van Duijn, and R.J. Schotting, Simulation of coning in bottom water-driven reservoirs, *Transport Porous Media*, **6** (1991), 35–69.
- [8] C.J. Coleman, D.L. Tullock, and N. Phan-Thien, An effective boundary element method for inhomogeneous partial differential equations, *Z. Angew. Math. Phys.*, **42** (1991), 730–745.
- [9] C. De Boor, Bicubic spline interpolation, *J. Math. Phys.*, **41** (1962), 212–218.
- [10] L.M. Delves and J.L. Mohamed, *Computational methods for integral equations*, (Cambridge University Press, Cambridge, 1985).
- [11] M.G. Duffy, Quadrature over a pyramid or cube of integrals with a singularity at a vertex, *SIAM J. Numer. Anal.*, **19** (1982), 1260–1262.
- [12] J.J.L. Higdon and G.P. Muldowney, A spectral boundary element approach for the three dimensional Stokes equations applied to free surface flows, *Boundary elements XVII*, edited by C.A. Brebbia, S. Kim, T.A. Osswald, and H. Power, (Computational Mechanics, Southampton, 1995).
- [13] E.J. Hinch, The recovery of oil from underground reservoirs, *PhysicoChemical Hydrodynamics*, **6** (1985), 601–622.
- [14] G.C. Hocking, Infinite Froude number solutions to the problem of a submerged source or sink, *J. Austral. Math. Soc.*, **B29** (1988), 401–409.
- [15] G.C. Hocking, Supercritical withdrawal from a two-layer fluid through a line sink, *J. Fluid Mech.*, **297** (1995), 37–47.

- [16] M. Iri, S. Moriguti and Y. Takasawa, On a certain quadrature formula, *J. Comput. Appl. Math.*, **17** (1987), 3–20.
- [17] D.K. Kahaner and O.W. Rechar, TWODQD, an adaptive routine for two-dimensional integration, *J. Comput. Appl. Math.*, **17** (1987), 215–234.
- [18] D.E. Knuth, *The Art of Computer Programming, Vol. 1, Fundamental Algorithms* (Addison-Wesley, Reading, MA, 1973).
- [19] J.C. Lachat and J.O. Watson, Effective numerical treatment of boundary integral equations: a formulation for three-dimensional elastostatics, *Int. J. Numer. Methods Eng.*, **10** (1976), 991–1005.
- [20] M.H. Lean and A. Wexler, Accurate numerical integration of singular boundary element kernels over boundaries with curvature, *Int. J. Numer. Methods Eng.*, **21** (1985), 211–228.
- [21] Y. Li, T. Obata, H. Koguchi, and T. Yada, Some improvements of accuracy and efficiency in three dimensional direct boundary element method, *Int. J. Numer. Methods Eng.*, **33** (1992), 1451–1464.
- [22] J.R. Lister, Selective withdrawal from a viscous two-layer system, *J. Fluid Mech.*, **198** (1989), 231–254.
- [23] S.K. Lucas, J.R. Blake and A. Kucera, A boundary-integral method applied to water coning in oil reservoirs, *J. Austral. Math. Soc.*, **B 32** (1991), 261–283.
- [24] J.F. McCarthy, Analytical solutions of 2D cresting models using the hodograph method, *Transport Porous Media*, **15** (1994), 251–269.
- [25] M. Muskat, *Physical Principles of Oil Production*, (McGraw-Hill, New York, 1949).
- [26] R. Piessens, E. De Donker-Kapenga, C.W. Uberhuber, and D.K. Kahauer, QUAD-PACK, *A Subroutine Package for Automatic Integration*, (Springer, Berlin, 1983).
- [27] M. Ramia, D.L. Tullock, and N. Phan-Thien, The role of hydrodynamic interaction in the locomotion of micro-organisms, *Biophys. J.*, **65** (1993), 755–778.
- [28] F.J. Rizzo and D.J. Shippy, An advanced boundary integral equation method for three-dimensional thermoelasticity, *Int. J. Numer. Methods Eng.*, **11** (1977), 1753–1768.
- [29] E.O. Tuck and J. Vanden-Broeck, A cusp-like free-surface flow due to a submerged source or sink, *J. Austral. Math. Soc.*, **B 25** (1984), 443–450.